



## Molecular Physics

An International Journal at the Interface Between Chemistry and Physics

ISSN: 0026-8976 (Print) 1362-3028 (Online) Journal homepage: <https://www.tandfonline.com/loi/tmph20>

# Evaluation of dynamical properties of open quantum systems using the driven Liouville-von Neumann approach: methodological considerations

Inbal Oz, Oded Hod & Abraham Nitzan

To cite this article: Inbal Oz, Oded Hod & Abraham Nitzan (2019) Evaluation of dynamical properties of open quantum systems using the driven Liouville-von Neumann approach: methodological considerations, Molecular Physics, 117:15-16, 2083-2096, DOI: [10.1080/00268976.2019.1584338](https://doi.org/10.1080/00268976.2019.1584338)

To link to this article: <https://doi.org/10.1080/00268976.2019.1584338>



Published online: 29 Mar 2019.



Submit your article to this journal [↗](#)



Article views: 80



View Crossmark data [↗](#)

NIMROD MOISEYEV



## Evaluation of dynamical properties of open quantum systems using the driven Liouville-von Neumann approach: methodological considerations

Inbal Oz<sup>a,b</sup>, Oded Hod<sup>a,b</sup> and Abraham Nitzan<sup>a,b,c</sup>

<sup>a</sup>Department of Physical Chemistry, School of Chemistry, The Raymond and Beverly Sackler Faculty of Exact Sciences, Tel Aviv University, Tel Aviv, IL, Israel; <sup>b</sup>The Sackler Center for Computational Molecular and Materials Science, Tel Aviv University, Tel Aviv, IL, Israel; <sup>c</sup>Department of Chemistry, University of Pennsylvania, Philadelphia, PA, USA

### ABSTRACT

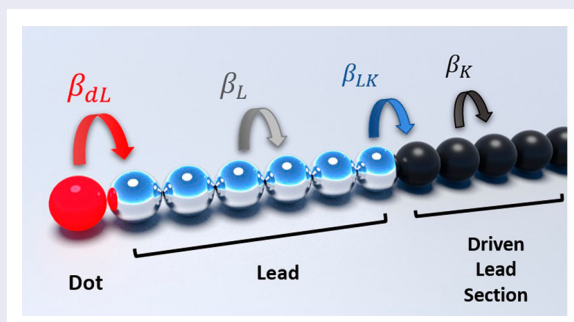
Methodological aspects of using the driven Liouville-von Neumann (DLvN) approach for simulating dynamical properties of molecular junctions are discussed. As a model system we consider a non-interacting resonant level uniformly coupled to a single Fermionic bath. We demonstrate how a finite system can mimic the depopulation dynamics of the dot into an infinite band bath of continuous and uniform density of states. We further show how the effects of spurious energy resolved currents, appearing due to the approximate nature of the equilibrium state obtained in DLvN calculations, can be avoided. Several ways to approach the wide band limit, which is often adopted in analytical treatments, using a finite numerical model system are discussed including brute-force increase of the lead model bandwidth as well as efficient cancellation or direct subtraction of finite-bandwidth effect. These methodological considerations may be relevant also for other numerical schemes that aim to study non-equilibrium thermodynamics via simulations of open quantum systems.

### ARTICLE HISTORY

Received 22 October 2018  
Accepted 10 February 2019

### KEYWORDS

Molecular junctions; molecular machines; driven Liouville-von Neumann approach; open quantum systems; quantum thermodynamics





## 1. Introduction

The study of electron dynamics and conductance in small electronic systems coupled to one or more free-electron reservoirs (each in its own equilibrium but not necessarily at equilibrium with each other) has attracted much attention over the past decade due to its importance for studies in the fields of molecular electronics [1–3], spectroscopy [4], and quantum thermodynamics [5–12]. Although substantial advances in observing and describing such processes were made in the past three decades, the study of particle and energy transfer in processes dominated by resonance transmission between non-equilibrium environments remains a major experimental

and theoretical challenge. As in other dynamical problems, computer simulations may offer a complementary approach to purely theoretical analysis in this field.

A major challenge for modelling electronic transport through such nanometric structures is the ability to provide an appropriate non-equilibrium description of the entire (infinite in principle) system. This problem is often solved by replacing the full system by a finite system with proper account of the non-equilibrium open boundaries. One of the most widely used approaches to address this challenge is the extension of the Landauer formalism to address dynamical effects by using the non-equilibrium Green's function method [13]. This method can provide

**CONTACT** Abraham Nitzan  [nitzan@post.tau.ac.il](mailto:nitzan@post.tau.ac.il)  Department of Physical Chemistry, School of Chemistry, The Raymond and Beverly Sackler Faculty of Exact Sciences, Tel Aviv University, Tel Aviv, IL 6997801, Israel; The Sackler Center for Computational Molecular and Materials Science, Tel Aviv University, Tel Aviv, IL 6997801, Israel; Department of Chemistry, University of Pennsylvania, Philadelphia, PA 19103, USA

analytical solutions for non-interacting models [14–16] but it becomes computationally demanding for steady-states of more realistic model systems as well as for systems affected by time-dependent driving.

An alternative approach to describing electronic transport in such systems is the use of numerical simulations. Since simulated models are necessarily of finite size, ways of imposing the infinite (in principle) nature of the real system need to be devised. In vacuum scattering problems this is usually achieved by using absorbing boundary conditions [17]. When the environment of the simulated system consists of metallic leads with occupied electronic states, the numerical boundary has to account for both electron absorption and injection. A variety of methods, too extensive to detail herein, have been developed for this purpose considering both model Hamiltonians [18–29] and realistic model systems [15–16,30–41]. Among the latter, the recently proposed Driven Liouville-von Neumann (DLvN) approach [42–45], imposes the required boundary conditions by augmenting the Liouville-von Neumann (LvN) equation of motion with non-unitary source and sink terms. The latter drive each lead towards an equilibrium state determined by the chemical potential and electronic temperature of the implicit bath to which it is coupled [42–45]. When the driving enforces different equilibrium states on different leads, the DLvN method was shown to provide a reliable representation of the electronic transport problem, closely reproducing the Landauer formalism results at steady-state [42,44]. Furthermore, it was shown that, for non-interacting systems [46–48], the DLvN equation of motion can be recast into Lindblad form, thus it inherently preserves density matrix positivity [24,44,48]. Notably, within this approach, external dynamic perturbations such as alternating bias voltages, varying gate potentials, and time-dependent external fields may be readily imposed. These can drive the system out of its equilibrium or steady states [14] and invoke intriguing physical phenomena that are manifested in the dynamical properties of the system, beyond the scope of the well-established equilibrium thermodynamic theory.

A simplistic model that can demonstrate such effects is a resonant level model, where a single non-interacting spinless state (often referred to as a quantum dot) is coupled to a manifold of non-interacting spinless lead states. Here, shifting the position of the dot level with respect to the chemical potential of the lead states mimics the application of an external time-dependent gate potential on the dot. Recent analytical analysis of this model at the wide band limit (WBL) [49–51] enabled the calculation of thermodynamic functions to first order beyond the quasistatic (QS) limit. These were shown to fulfil the first and second laws of thermodynamics and reproduce

the equilibrium and weak coupling results in the appropriate limits [5]. Such treatments, however, often rely on perturbation theory and hence are limited to cases where a small parameter can be identified. Specifically, in the treatment mentioned above, the dot level driving rate was taken to be considerably smaller than the typical internal relaxation rate of the lead. Hence, to gain access to dynamical regions that are beyond the reach of current analytical treatments of this (and more complex) models, one can harness the numerical flexibility of the DLvN approach. Nevertheless, care should be taken with the practical implementation of the numerical simulation to ensure that the results, necessarily obtained for a finite lead model, faithfully represent the desired physical properties of an infinite environment at equilibrium. As general guidance, some rules of thumb have been introduced to assess the finite lead model size required to verify the validity of the Markovian approximation adopted in the DLvN approach [24,48]. When numerical convergence with respect to the finite lead model size is achieved its discrete spectrum mimics well the continuous density of state of the corresponding (semi-)infinite bath. However, when using numerical simulations to extend analytical models towards new dynamical regimes, one should also keep in mind that simplifying assumptions, such as the wide band approximation (WBA), which are often invoked in approximate analytical treatments, are not always readily transferable to the numerical calculation. The present manuscript addresses these and related methodological aspects of using numerical simulations in general and, in particular, the DLvN approach to complement analytical treatments in the study of particle and heat fluxes through molecular interfaces.

## 2. Relaxation dynamics

To set the stage for demonstrating important methodological aspects of using numerical schemes to simulate non-equilibrium scenarios, we consider first the simple relaxation dynamics of an initially occupied dot level coupled to an empty manifold of lead levels. The non-interacting Hamiltonian of the entire system is given by

$$\hat{H}(t) = \hat{H}_d(t) + \hat{H}_L + \hat{H}_V, \quad (1)$$

where  $\hat{H}_d(t) = \varepsilon_d(t)c_d^\dagger c_d$  is the Hamiltonian of the dot,  $\hat{H}_L = \sum_l \varepsilon_l c_l^\dagger c_l$  represents the lead section, and  $\hat{H}_V = \hat{V}_{dL} + \hat{V}_{Ld}$  is the dot/lead coupling term, where  $\hat{V}_{dL} = \sum_l (V_l d^\dagger c_l)$  and  $\hat{V}_{Ld} = \hat{V}_{dL}^\dagger$ . Here,  $\varepsilon_d(t)$  and  $\varepsilon_l$  are the energies of the dot and lead level  $l$ , respectively, and  $c_i^\dagger$  and  $c_i$  are the creation and annihilation operators for an

electron in level  $i = d, l$ . Note that, for the sake of simplicity, we have assumed that the only time-dependence in the Hamiltonian stems from shifts in the position of the dot level, with no effect on the lead levels and the lead-dot coupling terms. Naturally, within the numerical treatment discussed below, this simplifying assumption can be readily lifted.

## 2.1. Analytical solution

Under the WBA, where the manifold of lead states is assumed to be of infinite width with a uniform and continuous density of states,  $\rho$ , this model has a fully analytical solution. Upon uniformly coupling the isolated dot level to the manifold of lead states, its original delta-function shape,  $\delta(\varepsilon - \varepsilon_d)$ , broadens into a Lorentzian function of the form:

$$A(\varepsilon - \varepsilon_d; \Delta, \gamma) = \frac{1}{\pi} \frac{\hbar\gamma/2}{(\varepsilon - \varepsilon_d - \Delta)^2 + (\hbar\gamma/2)^2}. \quad (2)$$

Here,  $\hbar = h/(2\pi)$  is the reduced Plank's constant,  $\Delta$  represents the shift in the dot's level position due to the coupling to the lead, and  $\hbar\gamma$  is the level broadening due to its finite lifetime. The latter corresponds the leakage rate of particles from the dot to the lead manifold as given by Fermi's golden rule [52]:

$$\gamma(\varepsilon) = \frac{2\pi}{\hbar} \sum_l |V_l|^2 \delta(\varepsilon - \varepsilon_l), \quad (3)$$

which at the WBL, assuming an infinite lead band of constant density of states,  $\rho$ , and uniform coupling to the dot,  $V_l = V = \text{const.}$ , can be evaluated as:

$$\begin{aligned} \gamma^{\text{WBA}} &= \frac{2\pi}{\hbar} \int_{-\infty}^{\infty} |V_l|^2 \rho(\varepsilon_l) \delta(\varepsilon - \varepsilon_l) d\varepsilon_l \\ &= \frac{2\pi}{\hbar} |V|^2 \rho \int_{-\infty}^{\infty} \delta(\varepsilon - \varepsilon_l) d\varepsilon_l = \frac{2\pi}{\hbar} |V|^2 \rho. \end{aligned} \quad (4)$$

By virtue of the Fourier transform of its Lorentzian spectral function, the population of an initially occupied dot level ( $\psi(t=0) = d^\dagger|0\rangle$ ) decays exponentially with time into the empty manifold of lead levels ( $P_d(t) = |\langle \psi(t=0) | e^{-\frac{i}{\hbar} \hat{H}t} | \psi(t=0) \rangle|^2 = e^{-\gamma t}$ ) with a characteristic decay time of  $1/\gamma$  as indicated by the dashed black line in Figure 1.

## 2.2. Closed system numerical treatment

The most straightforward numerical approach to simulate this temporal behaviour of the dot's population is the microcanonical scheme [16]. Here, the infinite (in principle) system is represented by a finite model consisting of

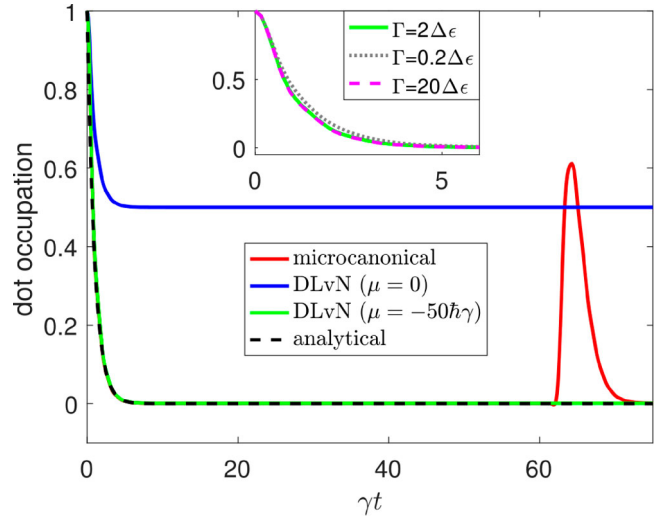


**Figure 1.** Dot depopulation dynamics as calculated using (i) the analytical WBA treatment (dashed black line); (ii) microcanonical simulations (full red line); (iii) DLvN simulations with an empty (green) and half filled (blue) lead. System parameters are provided in the main text. Inset: Driving rate sensitivity test of the DLvN dynamics calculated with  $\Gamma = 0.2\Delta\varepsilon/\hbar$  (dashed gray),  $\Gamma = 2\Delta\varepsilon/\hbar$  (green), and  $\Gamma = 20\Delta\varepsilon/\hbar$  (dashed magenta).

the dot level uniformly coupled to a finite set of lead levels. Two important differences between this model and the one used for the analytical treatment above should be noted: (i) the density of lead states is discrete, and (ii) the band of lead states is of finite width. Nevertheless, we expect that when the lead manifold is sufficiently dense and the position of the dot is far enough from the band edges, the numerical simulation will reproduce the short time dynamics of the analytical treatment. To demonstrate this, we choose a finite lead model consisting of  $N_L = 100$  equispaced levels that span a bandwidth of  $W = 10\hbar\gamma$ . The corresponding level spacing and density of states are thus given by  $\Delta\varepsilon = \rho^{-1} = \frac{W}{N} = 0.1\hbar\gamma$ , respectively. The dot energy,  $\varepsilon_d$ , is positioned at the centre of the lead's band and is uniformly coupled to all lead levels via a coupling constant of  $V = \sqrt{\frac{\hbar}{2\pi} \frac{\gamma}{\rho}} = \frac{\hbar\gamma}{\sqrt{20\pi}}$  (see Equation (4)). We note that, the choice of the specific value of  $\gamma$  (chosen herein such that  $\hbar\gamma = 0.1$  eV) is arbitrary as the results presented below are scalable with respect to it. Hence, we set all other parameters in terms of  $\gamma$  and present the results in unitless format. The dynamics of the system is simulated via the LvN equation of motion for the single-particle density matrix of the system,  $\hat{\sigma}(t)$ :

$$\frac{d}{dt} \hat{\sigma}(t) = -\frac{i}{\hbar} [\hat{H}(t), \hat{\sigma}(t)]. \quad (5)$$

In the basis of eigenstates of the dot and the lead sections of the system the density matrix obtains the

following block representation:

$$\hat{\sigma}(t) = \begin{pmatrix} \sigma_d(t) & \hat{\sigma}_{dL}(t) \\ \hat{\sigma}_{Ld}(t) & \hat{\sigma}_L(t) \end{pmatrix}, \quad (6)$$

whose elements are given by  $\sigma_{ij}(t) = \langle c_i(t)c_j^\dagger(t) \rangle$ . The corresponding block matrix representation of the Hamiltonian of Equation (1) is given by:

$$\hat{H}(t) = \begin{pmatrix} \varepsilon_d(t) & \hat{V}_{dL} \\ \hat{V}_{Ld} & \hat{H}_L \end{pmatrix}. \quad (7)$$

The initial diagonal density matrix represents a fully populated dot ( $\sigma_d(t=0) = 1$ ) and an empty lead ( $\hat{\sigma}_L(t=0) = \hat{0}$ ); In practice, we initially populate the lead levels according to a Fermi–Dirac distribution, whose chemical potential and temperature are set to  $\mu = -50\hbar\gamma$  and  $k_B T = 0.25\gamma$ , respectively). By monitoring the diagonal element of the density matrix that corresponds to the dot level we can follow its depopulation into the lead levels. The resulting dynamics, which is represented by the red curve in Figure 1, captures well the short-time ( $\gamma t < \gamma(\hbar\Delta\varepsilon^{-1}) = 20\pi$ , reflecting the highest frequency of the lead dynamics) exponential decay predicted by the analytical treatment. However, at longer timescales, characteristic Poincaré recurrences occur, reflecting the discrete nature of the quasi-continuum representation of the lead or, equivalently, the reflection of the scattered electron wavefunction from the far edge of the finite lead model [39,45–46,53–55]. Therefore, similar to previous multi-lead microcanonical transport calculations [16,36,42], it becomes evident that, while microcanonical simulations are not limited to the WBA, the finite closed system model can mimic the behaviour of its open counterpart only for times shorter than the typical reflection time-scale.

### 2.3. Driven Liouville-von Neumann simulations

As mentioned above, the recently developed DLvN approach can eliminate this limitation by expanding the capabilities of the microcanonical approach to simulate truly open quantum systems. Similar to previous multi-lead implementations of the DLvN approach [14,42–46,56], the LvN equation of motion for the single-lead setup considered herein is augmented by sink and source terms that absorb outgoing electrons (thus avoiding reflections) and inject thermalised electrons near the system boundaries, respectively, as follows:

$$\frac{d}{dt}\hat{\sigma}(t) = -\frac{i}{\hbar}[\hat{H}(t), \hat{\sigma}(t)] - \Gamma \begin{pmatrix} 0 & \frac{1}{2}\hat{\sigma}_{dL}(t) \\ \frac{1}{2}\hat{\sigma}_{Ld}(t) & \hat{\sigma}_L(t) - \hat{\sigma}_L^0 \end{pmatrix}. \quad (8)$$

The last term in Equation (8) serves to drive the lead section towards a target equilibrium state of the form  $\sigma_W^0 = \delta_W f_{FD}(\varepsilon_l; \mu, T)$ , where  $f_{FD}(\varepsilon_l; \mu, T) = [\exp((\varepsilon_l - \mu)/(k_B T)) + 1]^{-1}$  is the Fermi–Dirac equilibrium distribution with the chemical potential,  $\mu$ , and electronic temperature,  $T$ , of the electronic reservoir, to which the lead section is implicitly coupled, and  $k_B$  is Boltzmann’s constant. The density matrix obtained from Equation (8) is Hermitian, positive definite [44,48], and normalised such that  $\text{tr}[\hat{\sigma}(t)] = N_{tot}(t)$ , where  $N_{tot}(t)$  is the instantaneous total number of electrons in the system.

The driving rate,  $\Gamma$ , which can be extracted from the electronic properties of the implicit reservoir [45], represents the timescale on which thermal relaxation takes place in the lead, and is generally assumed to be fast relative to all other processes of interest. If, however, the lead’s driving rate is treated as a phenomenological parameter, one should make sure that the relaxation dynamics (i.e. the rate  $\gamma$ ) of the dot itself is insensitive to the choice of  $\Gamma$ . Since the latter broadens the lead levels, the  $\delta$ -functions appearing in Equation (3) for the dot’s relaxation rate should be replaced by the corresponding Lorentzian functions of the form  $L_l(\varepsilon - \varepsilon_l) = \frac{1}{\pi} \frac{\hbar\Gamma/2}{(\varepsilon - \varepsilon_l)^2 + (\hbar\Gamma/2)^2}$ , such that  $\gamma(\varepsilon) = 2\pi/\hbar \sum_l |V_l|^2 L_l(\varepsilon - \varepsilon_l)$ . If  $\hbar\Gamma \gg \Delta\varepsilon$  the summand is a smooth function of  $\varepsilon_l$ , which can be approximated by the following integral:

$$\gamma(\varepsilon) \approx \frac{2\pi}{\hbar} \int_{-W/2}^{W/2} |V(\varepsilon_l)|^2 \rho(\varepsilon_l) L_l(\varepsilon - \varepsilon_l) d\varepsilon_l. \quad (9)$$

Moreover, if  $|V(\varepsilon_l)|^2$  and  $\rho(\varepsilon_l)$  do not (or only weakly) depend on  $\varepsilon_l$  (in practice, a softer requirement that  $|V(\varepsilon_l)|^2 \rho(\varepsilon_l)$  is independent of  $\varepsilon_l$  is sufficient), they may be taken out of the integral, and if furthermore  $\hbar\Gamma \ll W$ , the limits of the remaining integral over  $L_l(\varepsilon - \varepsilon_l)$  can be safely taken to infinity yielding a value of 1 to a good approximation. Hence, the wide band result of Equation (4) stating that  $\gamma \approx (2\pi/\hbar)|V|^2\rho$  is recovered and the dynamics becomes independent of  $\Gamma$ . Thus, the lead model should be chosen sufficiently large and its energy band should be made sufficiently wide to allow for the value of  $\Gamma$  to fulfil the requirement  $\Delta\varepsilon \ll \hbar\Gamma \ll W$  [24,47,48], which assures that the finite lead model levels are sufficiently (but not over-)broadened to mimic the continuous density-of-state within the finite bandwidth of the corresponding bulk lead. We note in passing that the above considerations are not just technical, and have been repeatedly used to explain observations of molecular relaxation processes involving isolated (on relevant timescales) large molecules [57], where a discrete molecular spectrum appears (again on relevant timescales) to act as a continuum [5–8,58].

To demonstrate the performance of this approach for the case of a single-lead setup, we repeat the dot depopulation simulations of the previous section with the same model Hamiltonian using the DLvN equation of motion (8) with a driving rate of  $\hbar\Gamma = 2\Delta\varepsilon = 0.2\hbar\gamma$ , within the region spanned between  $\Delta\varepsilon = 0.1\hbar\gamma$  and  $W = 100\Delta\varepsilon = 10\hbar\gamma$ . The green curve in Figure 1 presents the dot population as a function of time obtained with the same initial conditions as those used in the microcanonical simulation described above and a target equilibrium lead density matrix of  $\sigma_{ll}^0 = \delta_{ll} f_{FD}(\varepsilon_l, \mu = -50\hbar\gamma, T = 0.25\hbar\gamma/k_B)$ . Clearly, the DLvN dynamics is able to reproduce both the short- and the long-term analytical exponential decay of the dot population, while eliminating the recurrences appearing in the microcanonical simulations. Thus, it is shown that the DLvN effectively couples the closed system to an external implicit bath resulting in a characteristic open quantum system dynamics. Furthermore, when setting the implicit bath's chemical potential at the centre of the lead band and equal to the dot's energy (both in the initial conditions and via the target lead equilibrium density matrix,  $\sigma_{ll}^0 = \delta_{ll} f_{FD}(\varepsilon_l, \mu = 0, T = 0.25\hbar\gamma/k_B)$ ), the dot equilibrates to the expected half-filled state (see blue line in Figure 1). In order to verify that our results are insensitive to the choice of driving rate we have repeated the empty lead calculations for  $\hbar\Gamma = 0.2\Delta\varepsilon$  and  $\hbar\Gamma = 20\Delta\varepsilon$ . The comparison, presented in the inset of Figure 1, clearly demonstrates the weak dependence of the simulated dynamics on the value of  $\Gamma$ . Notably, this holds true also for the lower value chosen, which is outside the validity range discussed above. This further demonstrates that, with appropriate choice of model parameters, the DLvN approach can effectively mimic different environmental conditions and may constitute an effective numerical scheme to complement analytical treatments in parameter regimes beyond their limiting assumptions.

### 3. Equilibrium currents

The simple single-lead model system discussed above demonstrated how the DLvN approach can capture the *total* current flowing between the dot level and the lead manifold which, according to the analytical treatment, is given by  $J(t) = -dP_d(t)/dt = \gamma e^{-\gamma t}$ . However, in many applications, especially when evaluating thermodynamics properties, it is useful to consider not only overall currents of given observables but also their resolution with respect to other observables. For example, the total current can be written in terms of its energy resolved components as  $J = \int j(\varepsilon)d\varepsilon$ , where  $j(\varepsilon)$  is the net particle flux per unit energy interval leaving the dot at a

given energy  $\varepsilon$ . The latter can be then used to evaluate thermodynamic quantities, such as the energy flux,  $J_E = \int j(\varepsilon)d\varepsilon$ , carried by the particles from the dot to the lead and the total heat flux that they will produce in the environment when they eventually get equilibrated in the lead,  $J_Q = \int d\varepsilon(\varepsilon - \mu)j(\varepsilon)$ .

Such energy resolved currents can be evaluated via the numerical solution of Equation (8), where the temporal variation of the occupation of lead level  $l$  is given by (see Appendix A):

$$\frac{d\sigma_{ll}(t)}{dt} = \frac{2}{\hbar} \Im(V_{ld}\sigma_{dl}(t)) - \Gamma(\sigma_{ll}(t) - \sigma_{ll}^0). \quad (10)$$

We may now identify the first term on the right-hand-side of Equation (10) as the incoming particle flux from the dot into lead level  $l$  and the second term as the corresponding outgoing flux into the implicit bath. Neglecting the broadening of the lead levels due to their coupling to the bath and to the dot, the former can be used to evaluate the energy resolved particle currents leaving the dot towards the lead at energy  $\varepsilon_l$ :

$$J_{dL}(\varepsilon_l, t) = \frac{2}{\hbar} \Im(V_{ld}\sigma_{dl}(t)), \quad (11)$$

and the latter approximates the particle flux leaving the lead into the implicit bath at the same energy:

$$J_{LB}(\varepsilon_l, t) = \Gamma(\sigma_{ll}(t) - \sigma_{ll}^0). \quad (12)$$

At equilibrium, we expect the total current and all of its energy resolved components to vanish. Nevertheless, within the DLvN approach, only the lead sections are directly equilibrated with their respective implicit baths. This is essential for simulating non-equilibrium scenarios. Therefore, since equilibration is not performed in the diagonal basis of the entire finite model system and the dot section is not explicitly equilibrated, for any finite lead model equilibrium can only be reached approximately. As a result, when setting  $d\hat{\sigma}/dt = 0$  in Equation (8) for the single-lead setup considered herein (this can be readily done by solving a Sylvester equation [24] as detailed in Appendix B), non-zero dot-lead coherences  $\sigma_{d,l}$  appear in the density matrix that lead to spurious non-vanishing energy resolved equilibrium currents. This, is clearly manifested by the red curve in Figure 2 showing the equilibrium energy resolved currents obtained for a lead model consisting of 50 equispaced levels that are spanning a bandwidth of  $W = 10\hbar\gamma$ . The lead levels, which are coupled to the dot via  $V = \sqrt{\frac{\hbar}{2\pi}} \frac{\gamma}{\rho} = \frac{\hbar\gamma}{\sqrt{10\pi}}$ , are driven at a rate of  $\Gamma = 0.4\gamma$  towards an equilibrium Fermi Dirac population with chemical potential of  $\mu = 0$  and electronic temperature of  $T = \frac{0.25\hbar\gamma}{k_B}$ . The highest absolute current value appears at the dot position of

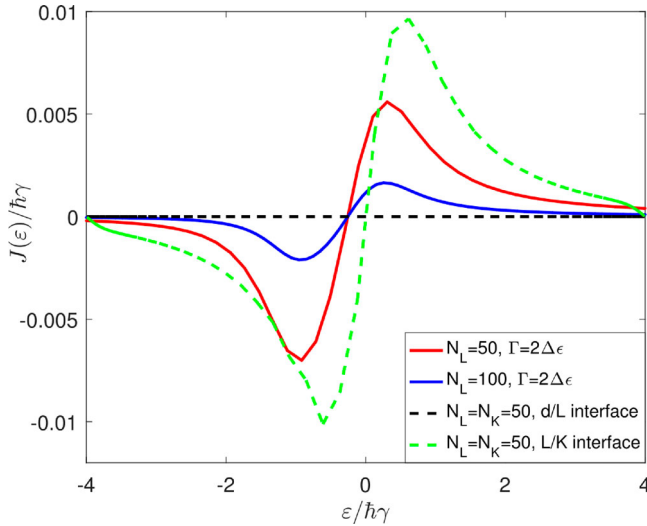


**Figure 2.** Spurious energy resolved equilibrium particle currents flowing between the dot and the various levels of a driven lead of  $N_L = 50$  (full red line) and  $N_L = 100$  (full blue line) levels, to which it is directly coupled. For a system composed of a dot, a lead of  $N_L = 50$  levels, and a driven-lead of  $N_K = 50$  levels the equilibrium energy resolved currents at the interface between the dot and the lead vanish (dashed black line), while those at the interface between the lead and the driven lead remain (dashed green line).

$\varepsilon_d = -\hbar\gamma$ . Notably, the total dot-lead current at equilibrium, obtained by summing over all its energy resolved equilibrium components,  $J_{dL} = \sum_l J_{dL}^{eq}(\varepsilon_l)$ , vanishes as expected. Nevertheless, the appearance of spurious non-vanishing energy resolved equilibrium currents jeopardises their validity for calculating non-equilibrium thermodynamic properties, such as energy and heat fluxes.

One remedy for this problem can be found by increasing the finite lead model size. At the limit of an

infinite lead, its spectrum mimics well that of the entire dot + lead system and the effect of not directly equilibrating the single dot level with the implicit bath becomes negligible. This is demonstrated in Figure 2, where doubling the number of lead levels from 50 (red) to 100 (blue), while keeping the bandwidth at  $W = 10\hbar\gamma$  (yielding  $\Delta\varepsilon = \rho^{-1} = 0.1\hbar\gamma$ ,  $V = \frac{\hbar\gamma}{\sqrt{20\pi}}$ , and  $\Gamma = 2\Delta\varepsilon/\hbar = 0.2\gamma$ ), reduces the magnitude of the energy-resolved equilibrium currents. The effects of any residual artificial currents on the calculation of non-equilibrium thermodynamic properties can be eliminated by subtracting their equilibrium contribution from the calculated dynamic properties.

Alternatively, an ‘extended-molecule’ strategy can be adopted. Here, the system is divided into three (rather than two as before) sections including (see left panel of Figure 3): (i) the dot ( $d$ ); (ii) the lead section adjacent to the dot that is directly coupled to it ( $L$ ); and (iii) a driven lead section ( $K$ ). The first two constitute the extended-dot section that is not directly coupled to the implicit bath. This buffers the dot from the effects of the open boundary conditions that are imposed only on the remote driven lead section. All physical quantities of interest can now be evaluated from the dynamics of the dot section and the dot/lead interface, where energy-resolved equilibrium currents vanish. To demonstrate this, we consider a tight-binding chain consisting of  $N_{tot} = 101$  sites, where the leftmost site serves as the dot, the  $N_L = 50$  sites adjacent to the dot form the lead section, and the remaining  $N_K = 50$  sites constitute the driven lead section. The onsite energies of the dot, the lead, and the driven lead sites are taken to be  $\alpha_d = \alpha_l = \alpha_k = 0$  eV, respectively. The hopping integrals between the various lead sites ( $\beta_l$ ), between the rightmost lead

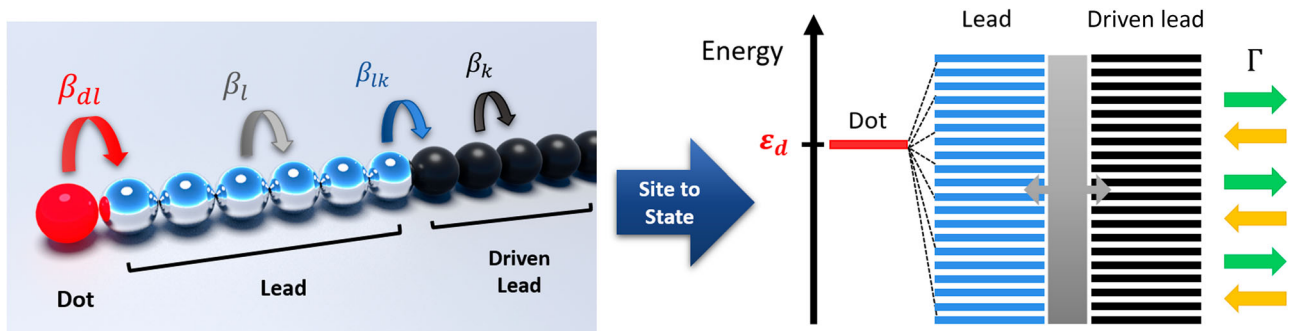


**Figure 3.** Site-to-state transformation. Left: Schematic site representation of the tight-binding model for a one dimensional chain composed of a dot (red), a lead (silver), and a driven-lead section (black).  $\beta_l$  and  $\beta_k$  denote the hopping integrals within the lead and the driven-lead sections, respectively.  $\beta_{dl}$  and  $\beta_{lk}$  are the coupling matrix elements between the dot and the leftmost site of the lead and between the rightmost site of the lead and the leftmost site of the driven-lead section, respectively. Right: Scheme of the single-particle state representation, where the dot level is uniformly coupled to the eigenstates of the lead section that are separately coupled to the manifold of eigenstates of the driven-lead section that, in turn, are equilibrated at a rate  $\Gamma$  with the implicit external bath.

site and leftmost driven lead site ( $\beta_{lk}$ ), and between the various driven lead sites ( $\beta_k$ ), are set to  $\beta_l = \beta_{lk} = \beta_k = 0.2$  eV, respectively. A weaker coupling of  $\beta_{ld} = 0.08$  eV is chosen between the dot and the leftmost site of the lead section and all other hopping integrals are nullified. This yields a (driven-)lead bandwidth of  $W_{(\text{driven-})\text{lead}} = 4\beta_{(k)l} = 0.8$  eV. The real-space tight-binding Hamiltonian matrix representation of the system can be written in block matrix form as follows:

$$\hat{H}(t) = \begin{pmatrix} \varepsilon_d(t) & \hat{V}_{dL} & \hat{0} \\ \hat{V}_{Ld} & \hat{H}_L & \hat{V}_{LK} \\ \hat{0} & \hat{V}_{KL} & \hat{H}_K \end{pmatrix}. \quad (13)$$

Here, the non-zero blocks are

$$\begin{aligned} \varepsilon_d(t) &= \alpha_d; \quad \hat{V}_{dL} = \hat{V}_{Ld}^\dagger = (\beta_{ld} \quad 0 \quad \dots); \\ \hat{H}_{L(K)} &= \begin{pmatrix} \alpha_{l(k)} & \beta_{l(k)} & 0 \\ \beta_{l(k)} & \alpha_{l(k)} & \ddots \\ 0 & \ddots & \ddots \end{pmatrix}; \\ \hat{V}_{LK} = \hat{V}_{KL}^\dagger &= \begin{pmatrix} \vdots & \vdots & \ddots \\ 0 & 0 & \dots \\ \beta_{lk} & 0 & \dots \end{pmatrix}. \end{aligned} \quad (14)$$

Giving dimensions of  $1 \times N_L$  for  $\hat{V}_{dL} = \hat{V}_{Ld}^\dagger$ ,  $N_{L(K)} \times N_{L(K)}$  for  $\hat{H}_{L(K)}$ , and  $N_L \times N_K$  for  $\hat{V}_{LK} = \hat{V}_{KL}^\dagger$ . In order to impose the DLvN boundary conditions on the eigenstates of the driven lead the following unitary ‘site-to-state’ transformation is performed (see Figure 3) [42]:

$$\hat{U} = \begin{pmatrix} 1 & \hat{0} & \hat{0} \\ \hat{0} & \hat{U}_L & \hat{0} \\ \hat{0} & \hat{0} & \hat{U}_K \end{pmatrix}, \quad (15)$$

where  $\hat{U}_L$  and  $\hat{U}_K$  are the unitary matrices that diagonalise  $\hat{H}_L$  and  $\hat{H}_K$ , respectively, such that  $\hat{H}_{L/K} = \hat{U}_{L/K}^\dagger \hat{H}_{L/K} \hat{U}_{L/K} = \text{diag}\{\varepsilon_{L/K}\}$ . The transformed Hamiltonian matrix has the same block structure as its real-space counterpart:

$$\hat{H}(t) = \hat{U}^\dagger \hat{H}(t) \hat{U} = \begin{pmatrix} \varepsilon_d(t) & \hat{V}_{dL} & \hat{0} \\ \hat{V}_{Ld} & \hat{H}_L & \hat{V}_{LK} \\ \hat{0} & \hat{V}_{KL} & \hat{H}_K \end{pmatrix} \quad (16)$$

where  $\hat{V}_{dL} = \hat{V}_{Ld}^\dagger$  hold the couplings between the dot and the various lead levels and  $\hat{V}_{LK} = \hat{V}_{KL}^\dagger$  store the couplings between the latter and the different driven lead levels (see right panel of Figure 3). In order to mimic the simulation conditions used above, where the

dot is uniformly coupled to all lead levels, we replace all elements in  $\hat{V}_{dL}$  (and  $\hat{V}_{Ld}^\dagger$ ) by their highest value of  $V \simeq 0.0158$  eV constituting the maximum of the corresponding Newns Anderson coupling band [43]. Given the density of lead states,  $\rho = 50/(4\beta_l) = 62.5$  eV<sup>-1</sup>, this yields  $\hbar\gamma = 0.0985$  eV (see Equation (4) above), which is comparable to the value of 0.1 eV used above.

The resulting DLvN equation of motion, written in the basis of eigenstates of the dot, lead, and driven lead sections, has the form:

$$\begin{aligned} \frac{d}{dt} \hat{\sigma}(t) &= -\frac{i}{\hbar} [\hat{H}(t), \hat{\sigma}(t)] \\ &- \Gamma \begin{pmatrix} 0 & \hat{0} & \frac{1}{2} \hat{\sigma}_{dK}(t) \\ \hat{0} & \hat{0} & \frac{1}{2} \hat{\sigma}_{LK}(t) \\ \frac{1}{2} \hat{\sigma}_{Kd}(t) & \frac{1}{2} \hat{\sigma}_{KL}(t) & \hat{\sigma}_K(t) - \hat{\sigma}_K^0 \end{pmatrix}, \end{aligned} \quad (17)$$

where  $\hat{\sigma}_K^0$  is the target equilibrium density matrix imposed by the implicit bath on the driven-lead section with  $\mu = 0$  and  $k_B T = 0.25\hbar\gamma$  and the driving rate is chosen as  $\Gamma = 2/(\hbar\rho) = 0.0486$  fs<sup>-1</sup>. When setting  $d\hat{\sigma}/dt = 0$  (see Appendix B), the energy resolved currents between the dot and the lead section now vanish (see dashed black curve in Figure 2) as required. Nevertheless, the equilibrium state of the entire finite system remains approximate and the spurious currents have been just driven away toward the (less physically relevant) interface between the lead and the driven lead sections. This is demonstrated by the dashed green curve in Figure 2, where we plot the total current flowing from the lead section to the various driven lead levels,  $k$ , calculated via

$$I_{LK}(\varepsilon_k) = \frac{2}{\hbar} \sum_l^{N_L} \Im(H_{kl} \sigma_{lk}(t)). \quad (18)$$

This, therefore, clearly demonstrates that care should be exercised when utilising numerical schemes using finite models to simulate (thermo)dynamic properties of open quantum systems. Brute force application of such schemes may lead to unphysical results that are strongly influenced by the applied boundary conditions.

#### 4. Finite bandwidth effects

The numerical examples provided above considered a static dot level placed sufficiently far from the lead’s band-edges and situated symmetrically between them. In non-equilibrium thermodynamic calculations, however, we will often be interested in simulating time-dependent perturbations applied to the system. These may include time-dependent external fields or varying gate potentials



that dynamically shift the dot's level energy. In such cases, it may become inevitable to position the dot level in the vicinity of the lead's band edges. Hence, it is important to understand both the physical and the numerical implications of approaching the band-edges of the modelled environment. This is especially true in the context of comparisons with, and extensions of, analytical treatments that, as stated above, often make simplifying assumptions, such as the WBA (see Sec. 3 above) that treats the environment as an infinite energy band of uniform and continuous density-of-states.

To demonstrate this, we study the changes in equilibrium total number of particles and electronic energy of the finite system upon shifting the dot away from the band center towards the upper band edge. Comparing the results for increasing band-widths to the predictions of the analytical WBA treatment allows us to assess the importance of band-edge effects and the convergence of the numerical model to the WBL. To this end, we consider the isolated system consisting of the dot level and a finite lead manifold of  $N_l$  states. We choose a uniform density of lead levels of  $\rho = 10(\hbar\gamma)^{-1}$  that are uniformly coupled to the dot level via  $V = \sqrt{\frac{\hbar\gamma}{2\pi\rho}} = \frac{\hbar\gamma}{\sqrt{20\pi}}$  (see Equation (3)). The dot level is first positioned at the center of the lead levels band,  $\varepsilon_d = 0$ , and the Hamiltonian matrix of the entire closed system is diagonalised. The eigenstates are then occupied according to the Fermi-Dirac distribution and the equilibrium number of particles and total electronic energy are calculated as:

$$N(\varepsilon_d = 0, W) = \sum_{j=0}^{N_l+1} f_{FD}(\varepsilon_j; \mu = 0, T = 0.25\hbar\gamma/k_B) \quad (19)$$

and

$$E(\varepsilon_d = 0, W) = \sum_{j=0}^{N_l+1} f_{FD}(\varepsilon_j; \mu = 0, T = 0.25\hbar\gamma/k_B) \varepsilon_j, \quad (20)$$

respectively, where  $W = N_l/\rho$ . Similarly, we obtain  $N(\varepsilon_d = 2\hbar\gamma, W)$  and  $E(\varepsilon_d = 2\hbar\gamma, W)$  by positioning the dot level  $2\hbar\gamma$  above the lead's band center, and calculate the variations  $\Delta N_{num}(W) = N(\varepsilon_d = 2\hbar\gamma, W) - N(\varepsilon_d = 0, W)$  and  $\Delta E_{num}(W) = E(\varepsilon_d = 2\hbar\gamma, W) - E(\varepsilon_d = 0, W)$ . To assess the correspondence between the numerical calculation and the analytical WBA results we repeat this procedure for increasing lead's bandwidth by increasing the number of lead states while keeping their density fixed. At the limit of infinite bandwidth we expect the numerical results to converge to the analytical WBA

values of:

$$\begin{aligned} \Delta N_{analytic} &= \int_{-\infty}^{\infty} [A(\varepsilon - 2\hbar\gamma; \Delta = 0; \gamma) - A(\varepsilon - 0; \Delta = 0; \gamma)] \\ &\quad \times f_{FD}(\varepsilon; \mu = 0, T = 0.25\hbar\gamma/k_B) d\varepsilon \end{aligned} \quad (21)$$

and

$$\begin{aligned} \Delta E_{analytic} &= \int_{-\infty}^{\infty} [A(\varepsilon - 2\hbar\gamma; \Delta = 0; \gamma) - A(\varepsilon - 0; \Delta = 0; \gamma)] \\ &\quad \times f_{FD}(\varepsilon; \mu = 0, T = 0.25\hbar\gamma/k_B) \varepsilon d\varepsilon. \end{aligned} \quad (22)$$

In practice, we calculate these integrals numerically with integration bounds of  $W = 3000\hbar\gamma$ , such that increasing the bounds to  $W = 3500\hbar\gamma$  gives a difference of 0.02% for the energy and  $9 \times 10^{-6}\%$  for the particle number. Note that when comparing the numerical results to the analytical values, the lead levels occupations are assumed to be insensitive to the dot level position such that  $\Delta N_{num}$  and  $\Delta E_{num}$  reflect only the change in dot occupation and energy contribution, like their analytical counterparts. Figure 4 shows the relative deviation of the change of number of particles (full blue line) with respect to the analytical WBA result  $\Delta\Delta N(W) = [\Delta N_{num}(W) - \Delta N_{analytic}]/\Delta N_{analytic}$  and the corresponding relative energy deviation (full red line)

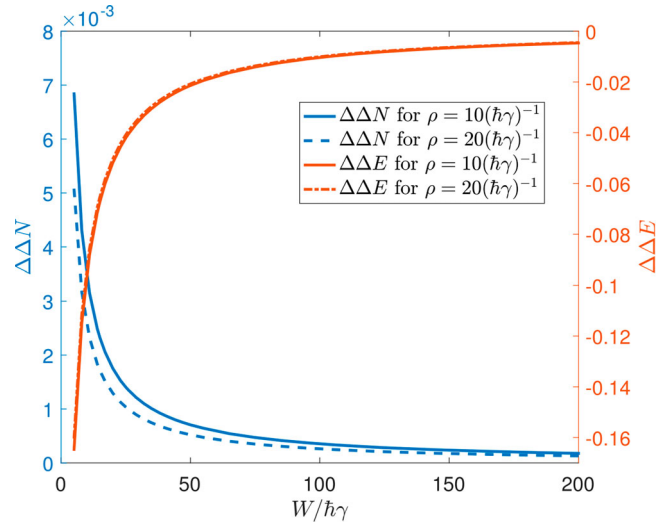


**Figure 4.** Convergence of the calculated equilibrium occupation,  $\Delta\Delta N$  (blue), and electronic energy,  $\Delta\Delta E$  (red), variations of the finite lead model system towards the wide band limit. The results are obtained for a density of lead states of  $\rho = 10(\hbar\gamma)^{-1}$  (full lines) and  $\rho = 20(\hbar\gamma)^{-1}$  (dashed lines).

$\Delta\Delta E(W) = [\Delta E_{num}(W) - \Delta E_{analytic}]/\Delta E_{analytic}$  as a function of bandwidth,  $W$ . We find that, for a finite band model, the change in number of particles upon the upshift of the dot level from the band center is larger than the analytical WBA result, whereas the corresponding change in electronic energy is smaller than its WBA counterpart. As expected, both  $\Delta N_{num}$  and  $\Delta E_{num}$  converge to the corresponding analytical WBL values with increasing finite lead model bandwidth. Notably, the particle number change converges faster than the electronic energy change, such that at a bandwidth of  $200\hbar\gamma$  the deviation of  $\Delta N_{num}$  from  $\Delta N_{analytic}$  reduces to 0.02%, while the corresponding deviation in the electronic energy is still larger than 0.5%. To rationalise this observation we note that the integrand of  $\Delta E_{analytic}$  includes  $\varepsilon$  itself, which diverges at the integration limits, and hence slows the convergence of the integrand at any finite integration range. This exemplifies a general behaviour that different observables converge at a different rate with system parameters, thus care should be taken to separately converge them. To further verify that these results are converged with respect to the choice of density of lead levels we have repeated the calculations for a density of  $\rho = 20(\hbar\gamma)^{-1}$  obtaining only minor deviations for the particle number and energy variations (see dashed blue and red lines in Figure 4, respectively). The analysis presented above thus demonstrates that numerical treatments can simulate various environment models ranging from simplistic wide-band baths to more complex finite-band baths that are not restricted to uniform density-of-states and/or system bath couplings.

The same holds true not only for simulating complex bath models but also for studying dynamical processes of the system itself. In the resonant level model discussed herein the latter may translate to dynamical shifts of the dot's level energy across the lead's band. Nevertheless, prior to performing dynamical simulations one should first verify that the numerical approach can reproduce quasi-static results. To this end, we repeated the procedure detailed above using a finite lead model consisting of 500 levels spanning a bandwidth of  $W = 10\hbar\gamma$ , which, according to Figure 4, reproduces WBA occupations and energetics down to  $\sim 0.4\%$  and  $\sim 9.5\%$ , respectively. The dot level is then uniformly coupled to all lead states with  $V = \frac{\hbar\gamma}{\sqrt{100\pi}}$  and its energy is varied around the chemical potential of the lead. For each dot level position,  $\varepsilon_d$ , the Hamiltonian of the entire finite model system is diagonalised and its eigenstates,  $\{|j\rangle\}$ , are occupied according to the equilibrium Fermi–Dirac distribution. As our observable we choose the dot section contribution to the total electronic energy of the system. In the above treatment we have assumed that the lead section

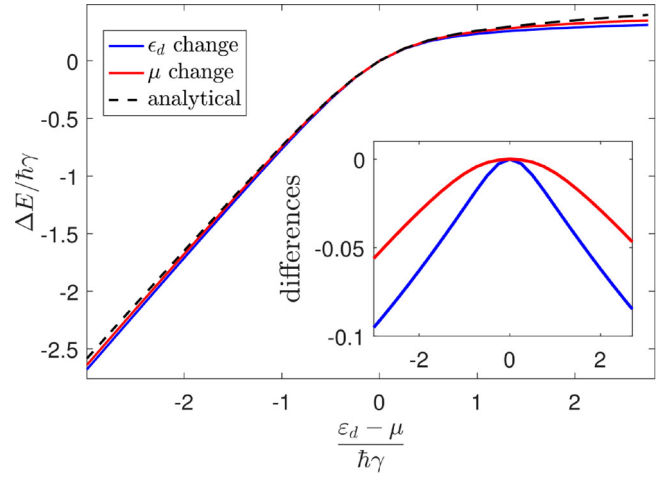


**Figure 5.** Comparison between the numerical evaluation (full blue and red lines) of the contribution to the total equilibrium electronic energy of a dot that is uniformly coupled to a discrete set of lead levels of finite bandwidth and the corresponding analytical WBA result (dashed black line). The numerical evaluation is performed either by shifting the dot's position while keeping the chemical potential fixed at the lead band center (blue) or vice versa (red). In all graphs, the Y-axis origin is set to the dot's contribution to the total energy when placed, along with the chemical potential, at the center of the lead's band. **Inset:** The differences between the numerical and the analytical evaluations of the dot's energy contribution to the total equilibrium electronic energy as a function of its position along the leads band. The line colours correspond to those in the main panel.

populations are insensitive to the dot level position, such that any change in total energy of the system reflects only the dot's contribution. Alternatively, we can evaluate it in the eigenbasis of the entire system via  $E_d^{num}(\varepsilon_d) = \sum_j \varepsilon_j f(\varepsilon_j) |\langle d|j\rangle|^2$ , where the sum runs over all eigenstates, and their individual contributions to the total electronic energy  $\varepsilon_j f(\varepsilon_j)$  ( $\varepsilon_j$  and  $f(\varepsilon_j)$  being the orbital energy and equilibrium occupation, respectively) are scaled by their projection on the dot section,  $|\langle d|j\rangle|^2$ . In Figure 5 we compare the numerical value (full blue line) obtained for  $\Delta E_d^{num}(\varepsilon_d) = E_d^{num}(\varepsilon_d) - E_d^{num}(\mu = 0)$  at various dot level positions in a range of  $\pm 2\hbar\gamma$  around the chemical potential (which is kept fix at  $\mu = 0$ ) and an electronic temperature of  $T = 0.25\hbar\gamma/k_B$ , to the analytical WBA results (dashed black line) obtained, as above, from:

$$\begin{aligned} \Delta E_d^{analytic}(\varepsilon_d) &= \int_{-\infty}^{\infty} [A(\varepsilon - \varepsilon_d; \Delta = 0; \gamma) - A(\varepsilon - \mu; \Delta = 0; \gamma)] \\ &\quad \times f_{FD}(\varepsilon; \mu = 0, T = 0.25\hbar\gamma/k_B) \varepsilon d\varepsilon. \end{aligned} \quad (23)$$

As noted above, in practice we calculate these integrals numerically with integration bounds of  $W = 3000\hbar\gamma$ . In the vicinity of the lead's Fermi energy the agreement between the two calculations is seen to be excellent. Minor deviations between the two develop as the dot position approaches the band edges of the finite lead model (see inset of Figure 5). To avoid such finite-bandwidth effects and achieve better agreement between the numerical results and the analytical wide band approximation we suggest an alternative approach, where the dot level is kept fixed at the lead's band center (symmetrically between the two band edges) and the chemical potential of the lead is varied around it. The results of this practice are presented by the full red line in Figure 5 showing better agreement with the analytical WBA results as is clearly demonstrated in the inset.

Having established that our method can reproduce quasi-static results we can now turn to discuss dynamic variations of the dot's level position. Simulating such processes with the closed system treatment presented above will require extremely large lead models to prevent backscattering from the finite-model boundaries during the relevant simulation time-scales. As demonstrated above, this can be readily avoided by using the DLvN approach, where broadening of the discrete manifold of levels of a relatively small finite lead model allows to mimic the continuous density-of-state of a (semi-)infinite bath. Results of such simulations can provide valuable dynamical information for finite band bath models. One might also wish to study, in the wide band limit, dynamical processes that cannot be accessed by current analytical treatments. Here, as well, we could increase the finite lead model until convergence with respect to its bandwidth is obtained. Within the context of dynamical simulations, however, this would considerably increase the computational burden and defeat the main purpose of the DLvN approach. Hence, again, we offer an alternative by assuming that the difference between the numerical finite-lead-band result and the analytical WBA results depend weakly on the rate of dot level shift. If this assumption is valid, we can extract this difference from a quasi-static calculation, where both numerical and analytical results are available:

$$\delta E_d(\varepsilon_d) = E_d^{num, QS}(\varepsilon_d) - E_d^{analytic, QS}(\varepsilon_d). \quad (24)$$

By subtracting this difference from the dynamic finite-bandwidth model numerical results we obtain an estimate of the corresponding WBL results. To demonstrate this, we use a relatively small lead model consisting of  $N_L = 100$  lead states spanning a bandwidth of  $W = 10\hbar\gamma$ . Notably, the latter is taken deliberately insufficient

to achieve convergence to the WBL (see Figure 4). We solve the DLvN equation of motion using a driving rate of  $\Gamma = 0.2\hbar\gamma$ , and a target density that provides a chemical potential of  $\mu = 0$  and an electronic temperature of  $T = \frac{0.25\gamma}{k_B}$ , starting at equilibrium with the dot level positioned at  $\varepsilon_d = \mu - 3\hbar\gamma$  and shifting it at a constant rate of  $\dot{\varepsilon}_d/(\hbar\gamma^2) = 0.6582$  up to  $\varepsilon_d = \mu + 3\hbar\gamma$ . Having the density matrix of the entire system at hand we can evaluate the temporal evolution of the dot's contribution to the total electronic energy using the following projection:

$$E_d^{num}(t) = \frac{1}{2} \langle d | \hat{H}(t) \hat{\sigma}(t) + \hat{\sigma}(t) \hat{H}(t) | d \rangle, \quad (25)$$

which is symmetrised to be real valued.

The results of this calculation (full blue line in Figure 6) differ from the quasi-static analytical WBA results (full red line in Figure 6) over the entire range of dot positions studied. This can be attributed to two main factors: (i) the finite lead bandwidth of the numerical model compared to the infinite bath band assumed in the analytical case; and (ii) the finite dot level shift rate used in the numerical simulation, which pushes the system out of its equilibrium state that is assumed by the quasi-static analytical treatment. Under the assumption mentioned above, we can eliminate the effect of the former by adding  $\delta E_d(\varepsilon_d(t)) = \delta E_d(\mu - 3\hbar\gamma + \dot{\varepsilon}_d t)$  to the calculated  $E_d^{num}(t)$ . This allows us to estimate effects of dynamical dot level shifts at the wide-band

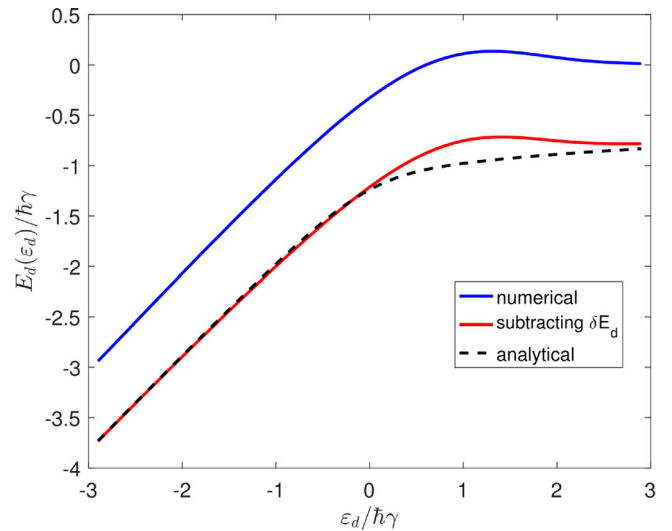


**Figure 6.** Dynamic contribution (full blue line) to the total electronic energy of a dot that is up-shifted at a finite rate across a discrete set of lead levels of finite bandwidth, to which it is uniformly coupled. Estimation of the corresponding WBL behaviour, obtained by subtracting  $\delta E_d(\varepsilon_d(t))$  from the simulation results, is presented in red. The quasi-static analytical WBA results are given as reference by the dashed black line.

bath limit. Comparing the red line in Figure 6 for  $E_d^{num,WBA}(t) = E_d^{num}(t) - \delta E_d(\varepsilon_d(t))$  to the dashed black line for  $E_d^{analytic,QS}(\varepsilon_d)$  we see that, up to the lead's Fermi energy the dynamical result resemble the quasi-static behaviour, exhibiting a linear increase. This reflects the fact that in this region the dot remains fully occupied and the variation of the dot's contribution to the total electronic energy stems only from changing its position. When approaching the Fermi level, the dot gradually empties into the lead. Hence the energy rise of  $E_d^{num,WBA}(t)$  due to the upshift of  $\varepsilon_d$  is countered by the dot's depopulation and its slope reduces. Noticeably, when the rate of the dot level up-shift becomes comparable or larger than  $\gamma$ , its emptying into the lead lags behind that of the quasi-static case. This results in the rate-dependent hysteresis evident in Figure 6, where  $E_d^{num,WBA}(t)$  overshoots  $E_d^{analytic,QS}(\varepsilon_d)$  in the vicinity of the lead Fermi energy. The analysis presented above thus demonstrates how DLvN based simulations can be used to study dynamical effects in open quantum systems in a wide range of system and bath parameters and extract important information relevant for evaluating their non-equilibrium thermodynamic properties.

## 5. Summary and Conclusions

The study of non-equilibrium dynamics and thermodynamics of open quantum systems is currently gaining increasing theoretical and experimental interest. Simple analytical treatments provide valuable insights regarding the extension of thermodynamic quantities towards non-equilibrium conditions. These, however, are often based on simplifying assumptions regarding the structure of the system, the environment, and their inter-coupling, thus limiting their validity to specific parameter ranges. Numerical approaches, such as the Driven Liouville-von Neumann methodology, can help bridge the gap between phenomenological analytical treatments and realistic experimental scenarios. In this paper, we presented a brief outline of the DLvN approach and discussed some important methodological aspects of its utilisation for studying non-equilibrium (thermo)dynamic properties. Specifically, we have demonstrated that DLvN simulations using finite model systems can capture the depopulation dynamics of an impurity electronic state uniformly coupled to an infinite bath of continuous and constant density of states. We have shown that when evaluating energy resolved quantities based on DLvN simulations, care should be taken to avoid the effects of spurious equilibrium currents resulting from the inherently approximate equilibrium state imposed

on the system. We have further studied the convergence of DLvN numerical simulations towards the wide band bath limit upon increasing the bandwidth of the finite lead model. Finally, we have shown how one can obtain reliable static and dynamic wide band results using relatively small model systems either via efficient cancellation of finite-bandwidth effect or by their direct subtraction from the simulated properties. Importantly, these methodological considerations may be relevant to other numerical techniques for simulating electron dynamics in open quantum systems. Hence, with the understanding gained herein, numerical approaches, such as the DLvN methodology, may become efficient tools for simulating non-equilibrium quantum thermodynamics in experimentally relevant regimes that are out of the reach of current analytical treatments.

## Acknowledgement

IO gratefully acknowledges the support of the Adams Fellowship Program of the Israel Academy of Sciences and Humanities, and the Naomi Foundation through the Tel-Aviv University GRTF Program. The research of AN is supported by the U.S. National Science Foundation [grant number CHE1665291], the Israel-U.S. Binational Science Foundation, the German Research Foundation (DFG TH 820/11-1), and the University of Pennsylvania. OH is grateful for the generous financial support of the Israel Science Foundation under [grant number 1740/13] and the Center for Nanoscience and Nanotechnology of Tel-Aviv University.

## Disclosure statement

No potential conflict of interest was reported by the authors.

## Funding

The research of AN is supported by the U.S. National Science Foundation (grant number CHE1665291), the Israel-U.S. Binational Science Foundation (grant number 2014113), the German Research Foundation (DFG TH 820/11-1), and the University of Pennsylvania. OH is grateful for the generous financial support of the Israel Science Foundation under grant number 1740/13 and the Center for Nanoscience and Nanotechnology of Tel-Aviv University. IO gratefully acknowledges the support of the Adams Fellowship Program of the Israel Academy of Sciences and Humanities, and the Naomi Foundation through the Tel-Aviv University GRTF Program.

## References

- [1] A. Nitzan and M.A. Ratner, *Science*. **300** (5624), 1384–1389 (2003).
- [2] J.C. Cuevas and E. Scheer, *Molecular Electronics: An Introduction to Theory and Experiment* (World Scientific, 2010).
- [3] A. Ghosh, *Nanoelectronics A Molecular View* (World Scientific, 2016).
- [4] M. Galperin and A. Nitzan, *Phys. Chem. Chem. Phys.* **14** (26), 9421–9438 (2012).

- [5] A. Bruch, M. Thomas, S. Viola Kusminskiy, F. von Oppen and A. Nitzan, *Phys. Rev. B* **93** (11), 115318 (2016).
- [6] M.F. Ludovico, J.S. Lim, M. Moskalets, L. Arrachea and D. Sánchez, *Phys. Rev. B* **89** (16), 161306(R) (2014).
- [7] M.F. Ludovico, M. Moskalets, D. Sánchez and L. Arrachea, *Phys. Rev. B* **94** (3), 035436 (2016).
- [8] M. Esposito, M. A. Ochoa, and M. Galperin, *Phys. Rev. Lett.* **114** (8), 080602 (2015).
- [9] R. Tuovinen, N. Säkkinen, D. Karlsson, G. Stefanucci, and R. van Leeuwen, *Phys. Rev. B* **93** (21), 214301 (2016).
- [10] D. Gelbwaser-Klimovsky, W. Niedenzu, and G. Kurizki, in *Atomic, Molecular, and Optical Physics* (Elsevier, 2015).
- [11] L. Arrachea, E.R. Mucciolo, C. Chamon and R.B. Capaz, *Phys. Rev. B* **86** (12), 125424 (2012).
- [12] R. Kosloff and A. Levy, *Annu. Rev. Phys. Chem.* **65** (1), 365–393 (2014).
- [13] H. Haug and A.-P. Jauho, *Quantum Kinetics in Transport and Optics of Semiconductors*, 2nd ed., vol. 123 (Springer-Verlag Berlin Heidelberg, 2008).
- [14] L. Chen, T. Hansen and I. Franco, *J. Phys. Chem. C* **118** (34), 20009–20017 (2014).
- [15] C.-L. Cheng, J.S. Evans and T. Van Voorhis, *Phys. Rev. B* **74** (15), 155112 (2006).
- [16] M. Di Ventura and T.N. Todorov, *J. Phys. Condens. Matter* **16** (45), 8025–8034 (2004).
- [17] T. Seideman and W.H. Miller, *J. Chem. Phys.* **96** (6), 4412–4422 (1992).
- [18] R. Baer and R. Kosloff, *J. Chem. Phys.* **106** (21), 8862–8875 (1997).
- [19] C.P. Koch, T. Klüner, H.-J. Freund and R. Kosloff, *Phys. Rev. Lett.* **90** (11), 117601 (2003).
- [20] M. Galperin and A. Nitzan, *Phys. Rev. Lett.* **95** (20), 206802 (2005).
- [21] U. Kleinekathöfer, G. Li, S. Welack and M. Schreiber, *Europhys. Lett. EPL* **75** (1), 139–145 (2006).
- [22] B.D. Fainberg, M. Jouravlev and A. Nitzan, *Phys. Rev. B* **76** (24), 245329 (2007).
- [23] G. Katz, D. Gelman, M.A. Ratner and R. Kosloff, *J. Chem. Phys.* **129** (3), 034108 (2008).
- [24] J.E. Subotnik, T. Hansen, M.A. Ratner and A. Nitzan, *J. Chem. Phys.* **130** (14), 144105 (2009).
- [25] A.E. Rothman and D.A. Mazziotti, *J. Chem. Phys.* **132** (10), 104112 (2010).
- [26] R. Volkovich and U. Peskin, *Phys. Rev. B* **83** (3), 033403 (2011).
- [27] N. Renaud, M.A. Ratner and C. Joachim, *J. Phys. Chem. B* **115** (18), 5582–5592 (2011).
- [28] U. Peskin and M. Galperin, *J. Chem. Phys.* **136** (4), 044107 (2012).
- [29] T.S. Nguyen, R. Nanguneri and J. Parkhill, *J. Chem. Phys.* **142** (13), 134113 (2015).
- [30] R. Baer and D. Neuhauser, *Int. J. Quantum Chem.* **91** (3), 524–532 (2003).
- [31] R. Baer, T. Seideman, S. Ilani and D. Neuhauser, *J. Chem. Phys.* **120** (7), 3387–3396 (2004).
- [32] N. Bushong, N. Sai and M. Di Ventura, *Nano Lett.* **5** (12), 2569–2572 (2005).
- [33] C. G. Sánchez, M. Stamenova, S. Sanvito, D. R. Bowler, A. P. Horsfield and T. N. Todorov, *J. Chem. Phys.* **124** (21), 214708 (2006).
- [34] X. Zheng, F. Wang, C.Y. Yam, Y. Mo and G. Chen, *Phys. Rev. B* **75** (19), 195127 (2007).
- [35] J. S. Evans and T. Van Voorhis, *Nano Lett.* **9** (7), 2671–2675 (2009).
- [36] I. Ercan and N.G. Anderson, *J. Appl. Phys.* **107** (12), 124318 (2010).
- [37] X. Zheng, G. Chen, Y. Mo, S. Koo, H. Tian, C. Yam and Y. Yan, *J. Chem. Phys.* **133** (11), 114101 (2010).
- [38] Y. Xing, B. Wang and J. Wang, *Phys. Rev. B* **82** (20), 205112 (2010).
- [39] S.-H. Ke, R. Liu, W. Yang and H.U. Baranger, *J. Chem. Phys.* **132** (23), 234105 (2010).
- [40] R. Wang, D. Hou and X. Zheng, *Phys. Rev. B* **88** (20), 205126 (2013).
- [41] P. Schaffhauser and S. Kümmel, *Phys. Rev. B* **93** (3), 035115 (2016).
- [42] T. Zelovich, L. Kronik and O. Hod, *J. Chem. Theory Comput.* **10** (8), 2927–2941 (2014).
- [43] T. Zelovich, L. Kronik and O. Hod, *J. Chem. Theory Comput.* **11** (10), 4861–4869 (2015).
- [44] T. Zelovich, L. Kronik and O. Hod, *J. Phys. Chem. C* **120** (28), 15052–15062 (2016).
- [45] T. Zelovich, T. Hansen, Z.-F. Liu, J.B. Neaton, L. Kronik and O. Hod, *J. Chem. Phys.* **146** (9), 092331 (2017).
- [46] O. Hod, C.A. Rodriguez-Rosario, T. Zelovich and T. Frauenheim, *J. Phys. Chem. A* **120** (19), 3278–3285 (2016).
- [47] D. Gruss, K.A. Velizhanin and M. Zwolak, *Sci. Rep.* **6** (1), 24514 (2016).
- [48] J.E. Elenewski, D. Gruss and M. Zwolak, *J. Chem. Phys.* **147** (15), 151101 (2017).
- [49] C.J.O. Verzijl, J.S. Seldenthuis and J.M. Thijssen, *J. Chem. Phys.* **138** (9), 094102 (2013).
- [50] I. Báldea, *Beilstein J. Nanotechnol.* **7**, 418–431 (2016).
- [51] F. Covito, F.G. Eich, R. Tuovinen, M.A. Sentef and A. Rubio, *J. Chem. Theory Comput.* **14** (5), 2495–2504 (2018).
- [52] A. Nitzan, *Chemical Dynamics in Condensed Phases: Relaxation, Transfer and Reactions in Condensed Molecular Systems* (OUP Oxford, 2006).
- [53] M. Koentopp, C. Chang, K. Burke and R. Car, *J. Phys. Condens. Matter* **20** (8), 083203 (2008).
- [54] S. Kurth, G. Stefanucci, C.-O. Almbladh, A. Rubio and E.K.U. Gross, *Phys. Rev. B* **72** (3), 035308 (2005).
- [55] M.A. Ochoa, A. Bruch and A. Nitzan, *Phys. Rev. B* **94** (3), 035420 (2016).
- [56] U.N. Morzan, F.F. Ramírez, M.C. González Lebrero and D.A. Scherlis, *J. Chem. Phys.* **146** (4), 044110 (2017).
- [57] M. Bixon and J. Jortner, *J. Chem. Phys.* **48** (2), 715–726 (1968).
- [58] B. Carmeli, R. Tulman, A. Nitzan and M.H. Kalos, *Chem. Phys.* **72** (3), 363–369 (1982).

## Appendix

### A. Energy resolved currents calculation

Energy resolved currents can be evaluated via the time derivatives of the various lead levels populations. Here, we show how the corresponding expression (Equation (11)) is obtained for the resonant level system discussed in the main text. For a system composed of a single dot level and a manifold of lead states that are directly coupled to an implicit bath (Equation (7)), the

DLvN equation of motion is given by the following matrix representation written in the basis of eigenstates of the isolated dot and lead sections (Equation (8)):

$$\begin{aligned} \frac{d}{dt} \begin{pmatrix} \sigma_d(t) & \hat{\sigma}_{dL}(t) \\ \hat{\sigma}_{Ld}(t) & \hat{\sigma}_L(t) \end{pmatrix} \\ = -\frac{i}{\hbar} \left[ \begin{pmatrix} \varepsilon_d(t) & \hat{V}_{dL} \\ \hat{V}_{Ld} & \hat{H}_L \end{pmatrix}, \begin{pmatrix} \sigma_d(t) & \hat{\sigma}_{dL}(t) \\ \hat{\sigma}_{Ld}(t) & \hat{\sigma}_L(t) \end{pmatrix} \right] \\ - \Gamma \begin{pmatrix} 0 & \frac{1}{2}\hat{\sigma}_{dL}(t) \\ \frac{1}{2}\hat{\sigma}_{Ld}(t) & \hat{\sigma}_L(t) - \hat{\sigma}_L^0 \end{pmatrix}. \end{aligned} \quad (\text{A1})$$

Evaluating the commutator on the right hand side of equation (A1), while taking into consideration that there is a single dot level, gives:

$$\begin{aligned} \frac{d}{dt} \begin{pmatrix} \sigma_d(t) & \hat{\sigma}_{dL}(t) \\ \hat{\sigma}_{Ld}(t) & \hat{\sigma}_L(t) \end{pmatrix} = -\Gamma \begin{pmatrix} 0 & \frac{1}{2}\hat{\sigma}_{dL}(t) \\ \frac{1}{2}\hat{\sigma}_{Ld}(t) & \hat{\sigma}_L(t) - \hat{\sigma}_L^0 \end{pmatrix} \\ - \frac{i}{\hbar} \left( \begin{array}{c} \hat{V}_{dL}\hat{\sigma}_{Ld}(t) - \hat{\sigma}_{dL}(t)\hat{V}_{Ld} \\ \hat{V}_{Ld}\hat{\sigma}_d(t) + \hat{H}_L\hat{\sigma}_{Ld}(t) - \hat{\sigma}_{Ld}(t)\varepsilon_d(t) - \hat{\sigma}_L(t)\hat{V}_{Ld} \\ \varepsilon_d(t)\hat{\sigma}_{dL}(t) + \hat{V}_{dL}\hat{\sigma}_L(t) - \sigma_d(t)\hat{V}_{dL} - \hat{\sigma}_{dL}(t)\hat{H}_L \\ \hat{V}_{Ld}\hat{\sigma}_{dL}(t) + \hat{H}_L\hat{\sigma}_L(t) - \hat{\sigma}_{Ld}(t)\hat{V}_{dL} - \hat{\sigma}_L(t)\hat{H}_L \end{array} \right) \end{aligned} \quad (\text{A2})$$

Hence, the dynamics of the lead section is given by:

$$\begin{aligned} \frac{d}{dt} \hat{\sigma}_L(t) = -\frac{i}{\hbar} [\hat{H}_L, \hat{\sigma}_L(t)] \\ - \frac{i}{\hbar} [\hat{V}_{Ld}\hat{\sigma}_{dL}(t) - \hat{\sigma}_{Ld}(t)\hat{V}_{dL}] - \Gamma(\hat{\sigma}_L(t) - \hat{\sigma}_L^0). \end{aligned} \quad (\text{A3})$$

From this we can calculate the rate of population variation in a given lead level  $l$  as:

$$\begin{aligned} \frac{d}{dt} \sigma_{ll}(t) = -\frac{i}{\hbar} \sum_{l'=0}^{N_l} [H_{ll'}\sigma_{l'l}(t) - \sigma_{ll'}(t)H_{l'l}] \\ - \frac{i}{\hbar} [V_{ld}\sigma_{dl}(t) - \sigma_{ld}(t)V_{dl}] - \Gamma(\sigma_{ll}(t) - \sigma_{ll}^0). \end{aligned} \quad (\text{A4})$$

In the representation of the eigenbasis of the isolated dot and lead states,  $\hat{H}_L$  is diagonal and thus the first term on the right hand side of equation (A4) vanishes. The remaining two terms can be identified as the particle current flowing between lead state  $l$  and the dot or the implicit bath, respectively. Focusing on the second term and taking into account the fact that  $\hat{H}$  and  $\hat{\sigma}$  are Hermitian matrices, such that  $V_{dl} = V_{ld}^*$  and  $\sigma_{ld}(t) = \sigma_{dl}^*(t)$ , we arrive at the expression for the current flowing from dot to lead level  $l$  (Equation (11) in the main text):

$$J_{dL}(\varepsilon_l, t) = -\frac{i}{\hbar} [V_{ld}\sigma_{dl}(t) - \sigma_{dl}^*(t)V_{ld}^*] = \frac{2}{\hbar} \Im(V_{ld}\sigma_{dl}(t)). \quad (\text{A5})$$

If we neglect the lead level width due to its coupling to the bath and the dot,  $J_{dL}(\varepsilon_l, t)$  represents the energy resolved current flowing from the dot to the lead at energy  $\varepsilon_l$ . Correspondingly, the particle current flowing at energy  $\varepsilon_l$  from the

lead to the implicit bath is given by (Equation (12) in the main text):

$$J_{LB}(\varepsilon_l, t) = \Gamma(\sigma_{ll}(t) - \sigma_{ll}^0). \quad (\text{A6})$$

The same holds true when the model system is decomposed into the dot, lead, and driven lead sections (Equation (13) in the main text), where equation (A1) remains valid for the current flowing between the dot and lead level  $l$ , and a similar expression is obtained for the current flowing from the lead into driven lead level  $k$ :

$$J_{LK}(\varepsilon_k, t) = \frac{2}{\hbar} \sum_{l=0}^{N_l} \Im(V_{kl}\sigma_{lk}(t)). \quad (\text{A7})$$

## B. Sylvester equation for the equilibrium density matrix

Within the DLvN approach, the equilibrium state of a single lead setup and the steady-state of a multi-lead setup can be obtained by setting  $\frac{d\hat{\sigma}(t)}{dt} = 0$ . As mentioned in the main text, for the former the obtained equilibrium is approximate as the equation of motion drives only the lead section, rather than the entire system (dot + lead) towards equilibrium. In principle, equilibrium can be reached by running the dynamics until all transient effects relax. This, however, may prove to be computationally quite inefficient, especially when the initial conditions are far from equilibrium. An alternative can be to formulate an equation that directly solves for  $\frac{d\hat{\sigma}(t)}{dt} = 0$  [24]. To this end, in the case of a single lead setup, we define projection operators on the dot and on the lead section as

$$\hat{P} = \begin{pmatrix} 1 & \hat{0} \\ \hat{0} & \hat{0} \end{pmatrix}, \hat{Q} = \begin{pmatrix} \hat{0} & \hat{0} \\ \hat{0} & \hat{1} \end{pmatrix}, \quad (\text{B1})$$

corresponding to the matrix representation in the basis of the isolated dot and lead eigenfunctions. With these, the driving term in Equation (8) in the main text can be decomposed as follows:

$$\begin{aligned} -\Gamma \begin{pmatrix} 0 & \frac{1}{2}\hat{\sigma}_{dL}(t) \\ \frac{1}{2}\hat{\sigma}_{Ld}(t) & \hat{\sigma}_L(t) - \hat{\sigma}_L^0 \end{pmatrix} \\ = -\frac{1}{2}\Gamma \underbrace{\begin{pmatrix} 0 & \hat{\sigma}_{dL}(t) \\ \hat{0} & \hat{0} \end{pmatrix}}_{\hat{P}\hat{\sigma}(t)\hat{Q}} - \frac{1}{2}\Gamma \underbrace{\begin{pmatrix} 0 & \hat{0} \\ \hat{\sigma}_{Ld}(t) & \hat{0} \end{pmatrix}}_{\hat{Q}\hat{\sigma}(t)\hat{P}} \\ - \Gamma \underbrace{\begin{pmatrix} 0 & \hat{0} \\ \hat{0} & \hat{\sigma}_L(t) \end{pmatrix}}_{\hat{Q}\hat{\sigma}(t)\hat{Q}} + \Gamma \underbrace{\begin{pmatrix} 0 & \hat{0} \\ \hat{0} & \hat{\sigma}_L^0 \end{pmatrix}}_{\hat{Q}\hat{\sigma}^0\hat{Q}}, \end{aligned} \quad (\text{B2})$$

where in the last term

$$\hat{\sigma}^0 = \begin{pmatrix} \sigma_d^0 & \hat{0} \\ \hat{0} & \hat{\sigma}_L^0 \end{pmatrix}, \quad (\text{B3})$$

and the target equilibrium occupation of the dot,  $\sigma_d^0$ , does not (and should not) appear in the final expression for the driving term. Nullifying the left hand side of the DLvN equation of motion (Equation (8)) with a time-independent Hamiltonian thus gives the following equation for the equilibrium density

matrix of the system,  $\hat{\sigma}^{eq}$ :

$$\begin{aligned} \frac{d}{dt}\hat{\sigma}^{eq} &= -\frac{i}{\hbar}\hat{H}\hat{\sigma}^{eq} + \frac{i}{\hbar}\hat{\sigma}^{eq}\hat{H} - \frac{1}{2}\Gamma\hat{P}\hat{\sigma}^{eq}\hat{Q} - \frac{1}{2}\Gamma\hat{Q}\hat{\sigma}^{eq}\hat{P} \\ &\quad - \Gamma\hat{Q}\hat{\sigma}^{eq}\hat{Q} + \Gamma\hat{Q}\hat{\sigma}^0\hat{Q} = \hat{0}, \end{aligned} \quad (B4)$$

which can be rearranged as:

$$\begin{aligned} &-\frac{i}{\hbar}\hat{H}\hat{\sigma}^{eq} + \frac{i}{\hbar}\hat{\sigma}^{eq}\hat{H} - \frac{1}{2}\Gamma(\hat{P} + \hat{Q})\hat{\sigma}^{eq}\hat{Q} \\ &\quad - \frac{1}{2}\Gamma\hat{Q}\hat{\sigma}^{eq}(\hat{P} + \hat{Q}) + \Gamma\hat{Q}\hat{\sigma}^0\hat{Q} = \hat{0}. \end{aligned} \quad (B5)$$

Since the sum of  $\hat{P}$  and  $\hat{Q}$  gives the unity matrix,  $\hat{1}$ , this results in:

$$\left(\frac{i}{\hbar}\hat{H} + \frac{1}{2}\Gamma\hat{Q}\right)\hat{\sigma}^{eq} - \hat{\sigma}^{eq}\left(\frac{i}{\hbar}\hat{H} - \frac{1}{2}\Gamma\hat{Q}\right) = \Gamma\hat{Q}\hat{\sigma}^0\hat{Q}. \quad (B6)$$

Defining

$$\hat{A} \equiv \frac{i}{\hbar}\hat{H} + \frac{1}{2}\Gamma\hat{Q} = \frac{i}{\hbar}\begin{pmatrix} \varepsilon_d & \hat{V}_{dL} \\ \hat{V}_{Ld} & \hat{H}_L - \frac{i\hbar}{2}\Gamma \end{pmatrix}, \quad (B7)$$

$$\hat{B} \equiv \frac{i}{\hbar}\hat{H} - \frac{1}{2}\Gamma\hat{Q} = \frac{i}{\hbar}\begin{pmatrix} \varepsilon_d & \hat{V}_{dL} \\ \hat{V}_{Ld} & \hat{H}_L + \frac{i\hbar}{2}\Gamma \end{pmatrix}, \quad (B8)$$

and

$$\hat{C} \equiv \Gamma\hat{Q}\hat{\sigma}^0\hat{Q} = \begin{pmatrix} 0 & \hat{0} \\ \hat{0} & \Gamma\hat{\sigma}_K^0 \end{pmatrix}, \quad (B9)$$

the following Sylvester equation for the equilibrium density matrix is obtained [24]:

$$\hat{A}\hat{\sigma}^{eq} - \hat{\sigma}^{eq}\hat{B} = \hat{C}. \quad (B10)$$

A similar Sylvester equation can be derived when the system is decomposed into the dot, lead, and driven lead sections. In the basis of eigenfunctions of these isolated sections the corresponding projection operators are written as:

$$\hat{P} = \begin{pmatrix} 1 & \hat{0} & \hat{0} \\ \hat{0} & \hat{0} & \hat{0} \\ \hat{0} & \hat{0} & \hat{0} \end{pmatrix}, \hat{Q} = \begin{pmatrix} 0 & \hat{0} & \hat{0} \\ \hat{0} & \hat{1} & \hat{0} \\ \hat{0} & \hat{0} & \hat{0} \end{pmatrix}, \hat{R} = \begin{pmatrix} 0 & \hat{0} & \hat{0} \\ \hat{0} & \hat{0} & \hat{0} \\ \hat{0} & \hat{0} & \hat{1} \end{pmatrix}. \quad (B11)$$

The driving term (see Equation (17)) can be decomposed in terms of these projection operators as follows:

$$\begin{aligned} &-\Gamma \begin{pmatrix} 0 & \hat{0} & \frac{1}{2}\hat{\sigma}_{dK}(t) \\ \hat{0} & \hat{0} & \frac{1}{2}\hat{\sigma}_{LK}(t) \\ \frac{1}{2}\hat{\sigma}_{Kd}(t) & \frac{1}{2}\hat{\sigma}_{KL}(t) & \hat{\sigma}_K(t) - \hat{\sigma}_K^0 \end{pmatrix} \\ &= -\frac{1}{2}\Gamma \underbrace{\begin{pmatrix} 0 & \hat{0} & \hat{0} \\ \hat{0} & \hat{0} & \hat{0} \\ \hat{\sigma}_{Kd}(t) & \hat{0} & \hat{0} \end{pmatrix}}_{\hat{R}\hat{\sigma}(t)\hat{P}} - \frac{1}{2}\Gamma \underbrace{\begin{pmatrix} 0 & \hat{0} & \hat{0} \\ \hat{0} & \hat{0} & \hat{0} \\ \hat{0} & \hat{\sigma}_{KL}(t) & \hat{0} \end{pmatrix}}_{\hat{R}\hat{\sigma}(t)\hat{Q}} \\ &= -\frac{1}{2}\Gamma \underbrace{\begin{pmatrix} 0 & \hat{0} & \hat{\sigma}_{dK}(t) \\ \hat{0} & \hat{0} & \hat{0} \\ \hat{0} & \hat{0} & \hat{0} \end{pmatrix}}_{\hat{P}\hat{\sigma}(t)\hat{R}} - \frac{1}{2}\Gamma \underbrace{\begin{pmatrix} 0 & \hat{0} & \hat{0} \\ \hat{0} & \hat{0} & \hat{\sigma}_{LK}(t) \\ \hat{0} & \hat{0} & \hat{0} \end{pmatrix}}_{\hat{Q}\hat{\sigma}(t)\hat{R}} \\ &= -\Gamma \underbrace{\begin{pmatrix} 0 & \hat{0} & \hat{0} \\ \hat{0} & \hat{0} & \hat{0} \\ \hat{0} & \hat{0} & \hat{\sigma}_K(t) \end{pmatrix}}_{\hat{R}\hat{\sigma}(t)\hat{R}} + \Gamma \underbrace{\begin{pmatrix} 0 & \hat{0} & \hat{0} \\ \hat{0} & \hat{0} & \hat{0} \\ \hat{0} & \hat{0} & \hat{\sigma}_K^0 \end{pmatrix}}_{\hat{R}\hat{\sigma}^0\hat{R}}, \end{aligned} \quad (B12)$$

where, in the last term,

$$\hat{\sigma}^0 = \begin{pmatrix} \sigma_d^0 & \hat{0} & \hat{0} \\ \hat{0} & \hat{\sigma}_L^0 & \hat{0} \\ \hat{0} & \hat{0} & \hat{\sigma}_K^0 \end{pmatrix}, \quad (B13)$$

and the target equilibrium occupation of the dot ( $\sigma_d^0$ ) and the lead ( $\sigma_L^0$ ) do not (and should not) appear in the final expression for the driving term. Nullifying the left hand side of the DLvN equation of motion (Equation (17)) with a time-independent Hamiltonian thus gives the following equation for the equilibrium density matrix of the system,  $\hat{\sigma}^{eq}$ :

$$\begin{aligned} \frac{d}{dt}\hat{\sigma}^{eq} &= -\frac{i}{\hbar}\tilde{H}\hat{\sigma}^{eq} + \frac{i}{\hbar}\hat{\sigma}^{eq}\tilde{H} - \frac{1}{2}\Gamma\hat{R}\hat{\sigma}^{eq}\hat{P} - \frac{1}{2}\Gamma\hat{R}\hat{\sigma}^{eq}\hat{Q} \\ &\quad - \frac{1}{2}\Gamma\hat{P}\hat{\sigma}^{eq}\hat{R} - \frac{1}{2}\Gamma\hat{Q}\hat{\sigma}^{eq}\hat{R} - \Gamma\hat{R}\hat{\sigma}^{eq}\hat{R} + \Gamma\hat{R}\hat{\sigma}^0\hat{R} = \hat{0} \end{aligned} \quad (B14)$$

which can be rearranged as:

$$\begin{aligned} &-\frac{i}{\hbar}\tilde{H}\hat{\sigma}^{eq} + \frac{i}{\hbar}\hat{\sigma}^{eq}\tilde{H} - \frac{1}{2}\Gamma\hat{R}\hat{\sigma}^{eq}(\hat{P} + \hat{Q} + \hat{R}) \\ &\quad - \frac{1}{2}\Gamma(\hat{P} + \hat{Q} + \hat{R})\hat{\sigma}^{eq}\hat{R} + \Gamma\hat{R}\hat{\sigma}^0\hat{R} = \hat{0}. \end{aligned} \quad (B15)$$

Since the sum of  $\hat{P} + \hat{Q} + \hat{R} = \hat{1}$  this results in:

$$\left(\frac{i}{\hbar}\tilde{H} + \frac{1}{2}\Gamma\hat{R}\right)\hat{\sigma}^{eq} - \hat{\sigma}^{eq}\left(\frac{i}{\hbar}\tilde{H} - \frac{1}{2}\Gamma\hat{R}\right) = \Gamma\hat{R}\hat{\sigma}^0\hat{R}. \quad (B16)$$

Defining

$$\hat{A} \equiv \frac{i}{\hbar}\tilde{H} + \frac{1}{2}\Gamma\hat{R} = \frac{i}{\hbar}\begin{pmatrix} \varepsilon_d & \tilde{V}_{dL} & \hat{0} \\ \tilde{V}_{Ld} & \tilde{H}_L & \tilde{V}_{LK} \\ \hat{0} & \tilde{V}_{KL} & \tilde{H}_K - \frac{i\hbar}{2}\Gamma \end{pmatrix}, \quad (B17)$$

$$\hat{B} \equiv \frac{i}{\hbar}\tilde{H} - \frac{1}{2}\Gamma\hat{R} = \frac{i}{\hbar}\begin{pmatrix} \varepsilon_d & \tilde{V}_{dL} & \hat{0} \\ \tilde{V}_{Ld} & \tilde{H}_L & \tilde{V}_{LK} \\ \hat{0} & \tilde{V}_{KL} & \tilde{H}_K + \frac{i\hbar}{2}\Gamma \end{pmatrix}, \quad (B18)$$

and

$$\hat{C} \equiv \Gamma\hat{R}\hat{\sigma}^0\hat{R} = \begin{pmatrix} 0 & \hat{0} & \hat{0} \\ \hat{0} & \hat{0} & \hat{0} \\ \hat{0} & \hat{0} & \Gamma\hat{\sigma}_K^0 \end{pmatrix}, \quad (B19)$$

we arrive at a Sylvester equation of the same structure as Equation (B10) above.